J Appl Physiol 93: 2070–2080, 2002.
First published August 23, 2002; 10.1152/japplphysiol.00129.2002.

Impact of axial diffusion on nitric oxide exchange in the lungs

HYE-WON SHIN[1] AND STEVEN C. GEORGE[1,2]
Departments of [1]Chemical Engineering and Materials Science and [2]Biomedical Engineering, University of California, Irvine, California 92697

Received 20 February 2002; accepted in final form 22 August 2002

Shin, Hye-Won, and Steven C. George. Impact of axial diffusion on nitric oxide exchange in the lungs. *J Appl Physiol* 93: 2070–2080, 2002. First published August 23, 2002; 10.1152/japplphysiol.00129.2002.—Nitric oxide (NO) appears in the exhaled breath and is a potentially important clinical marker. The accepted model of NO gas exchange includes two compartments, representing the airway and alveolar region of the lungs, but neglects axial diffusion. We incorporated axial diffusion into a one-dimensional trumpet model of the lungs to assess the impact on NO exchange dynamics, particularly the impact on the estimation of flow-independent NO exchange parameters such as the airway diffusing capacity and the maximum flux of NO in the airways. Axial diffusion reduces exhaled NO concentrations because of diffusion of NO from the airways to the alveolar region of the lungs. The magnitude is inversely related to exhalation flow rate. To simulate experimental data from two different breathing maneuvers, NO airway diffusing capacity and maximum flux of NO in the airways needed to be increased approximately fourfold. These results depend strongly on the assumption of a significant production of NO in the small airways. We conclude that axial diffusion may decrease exhaled NO levels; however, more advanced knowledge of the longitudinal distribution of NO production and diffusion is needed to develop a complete understanding of the impact of axial diffusion.

gas exchange; model; exhaled breath

NITRIC OXIDE (NO) is an important physiological mediator within the lungs and has potential clinical importance as a noninvasive marker of lung inflammation as well (2). However, NO exchange dynamics in the lungs are not yet fully developed, primarily because of the fact that exhaled NO has both airway and alveolar contributions (3, 5, 13, 21). Tsoukias and co-workers (24, 26) first combined experimental results with a two-compartment model in an attempt to describe both alveolar and airway sources. This was followed by similar models described by Pietropaoli et al. (12) and Silkoff et al. (23) as well as new breathing techniques that used the two-compartment model (17, 26) to characterize NO exchange dynamics. Use of the two-compartment model to enhance our understanding of a range of inflammatory diseases such as asthma (23), cystic fibrosis (18), and allergic alveolitis (8, 9) quickly followed.

The important feature of the two-compartment model is the partitioning of exhaled NO into airway and alveolar contributions and characterizing NO exchange with as few as three parameters that do not depend on the exhalation flow rate. These flow-independent parameters include the maximum flux of NO from the airways (J_{awNO}), the diffusing capacity of NO in the airways (D_{awNO}), and the steady-state alveolar concentration ($C_{A_{ss}}$). To maintain conceptual and mathematical simplicity, all of the models presented thus far have neglected axial diffusion in the gas phase and considered only convection of NO in the airways as a mode of transport. However, there is ample evidence in the literature suggesting that axial diffusion in the gas phase is an important gas-exchange mechanism, particularly in the very small airways and alveoli. Previous investigators have demonstrated that axial diffusion can play an important role in describing the washout of inert gases (He and SF_6) from the lungs, as well as the mechanisms underlying the positive slope of the alveolar plateau of CO_2 and N_2 (10, 11, 14, 15). NO contrasts with these other gases in that it has both an airway and an alveolar source. Thus the importance of axial diffusion on NO exchange dynamics has yet to be investigated. Because of the fact that NO has a source in the peripheral lung (where the relative impact of axial diffusion is greatest), we hypothesize that axial diffusion may play a role in NO gas exchange and affect the estimation of flow-independent NO exchange parameters.

The goal of this study is to assess the impact of axial diffusion on NO gas exchange and, in particular, on the estimation of the previously described flow-independent parameters. We developed a one-dimensional model ("trumpet model") of NO gas exchange based on the symmetrical bifurcating structure of Weibel (28). We evaluated the performance of the model in the presence and absence of axial diffusion by comparing it to experimental exhaled NO data in the literature. We conclude that axial diffusion may decrease the exhaled concentration of NO, and the relative importance is

Address for reprint requests and other correspondence: S. C. George, Dept. of Chemical Engineering and Materials Science, 916 Engineering Tower, Univ. of California, Irvine, Irvine, California 92697-2575 (E-mail: scgeorge@uci.edu).

The costs of publication of this article were defrayed in part by the payment of page charges. The article must therefore be hereby marked "*advertisement*" in accordance with 18 U.S.C. Section 1734 solely to indicate this fact.

inversely related to exhalation flow rate. The potential loss of NO in the exhaled breath may lead to an underestimation in both J_{awNO} and D_{awNO}; however, this result is strongly dependent on a significant production of NO in the small airways.

Glossary

$A_{I,II}$	Area under the curve in phases I and II of the exhaled NO profile, parts per billion (ppb)/s
A_{aw}	Total surface area of airway space, cm^2
$A_{c,aw}(z)$	Cross-sectional area of airway space, cm^2
$A_{c,A}$	Total cross-sectional area of alveolar space, cm^2
C_{NO}	Concentration of NO in the gas phase of the lungs, ppb
$C_{A_{ss}}$	Steady-state alveolar concentration of NO, ppb
C_{exh}	Exhaled NO concentration, ppb
C^*_{exh}	Model-predicted exhaled concentration, ppb
C_{NOplat}	Plateau exhaled NO concentration at a constant exhalation flow rate, ppb
D_{awNO}	Diffusing capacity (ml/s) of NO in the entire airway tree, which is expressed as the volume of NO per second per fractional concentration of NO in the gas phase [ml $NO \cdot s^{-1} \cdot$ (ml NO/ml gas)$^{-1}$] and is equivalent to $pl \cdot s^{-1} \cdot ppb^{-1}$
D'_{awNO}	Diffusing capacity of NO in the airway per unit axial distance, $ml \cdot s^{-1} \cdot cm^{-1}$
$D_{A_{NO}}$	Diffusing capacity (ml/s) of NO in the alveoli, which is expressed as the volume of NO per second per fractional concentration of NO in the gas phase [ml $NO \cdot s^{-1} \cdot$(ml NO/ml gas)$^{-1}$] and is equivalent to $pl \cdot s^{-1} \cdot ppb^{-1}$
$D'_{A_{NO}}$	Diffusing capacity of NO in the alveoli per unit axial distance, $ml \cdot s^{-1} \cdot cm^{-1}$
$D_{NO,air}$	Molecular diffusivity (diffusion coefficient) of NO in air, cm^2/s
J_{awNO}	Maximum total volumetric flux ($ppb \cdot ml \cdot s^{-1}$ or pl/s) of NO from the airways
J'_{awNO}	Maximum total volumetric flux of NO from the airways per unit axial distance, $ppb \cdot ml \cdot s^{-1} \cdot cm^{-1}$
$J_{A_{NO}}$	Maximum total volumetric flux ($ppb \cdot ml \cdot s^{-1}$ or pl/s) of NO from the alveoli
$J'_{A_{NO}}$	Maximum total volumetric flux of NO from the alveoli per unit axial distance, $ppb \cdot ml \cdot s^{-1} \cdot cm^{-1}$
L	Length of airway in trumpet model (27.40 cm)
$N(z)$	Number of alveoli per unit axial distance
N_t	Total number of alveoli
N_{max}	Maximum number of alveoli at any axial position
n_{III}	Number of data points in phase III of the exhalation profile
ρ	Molar density of the gas in the lungs (mol/cm^3); constant
RMS	Root-mean-square error between experimental data and model prediction
$\dot{V}_E$	Volumetric flow rate of air during expiration
z	Axial position in the lungs, cm

METHODS

Model development. The structure of the trumpet model used to describe both the airways and the alveolar region of the lungs is shown in Fig. 1*A* and is based on Weibel's anatomic data (28). We will reserve the term "two-compartment" model to describe the model previously reported to describe NO exchange dynamics (24) in which the alveolar region is a single well-mixed compartment and not distributed axially, as in the trumpet model described in this study. The following governing partial differential equation (additional details of the derivation presented in the APPENDIX), for

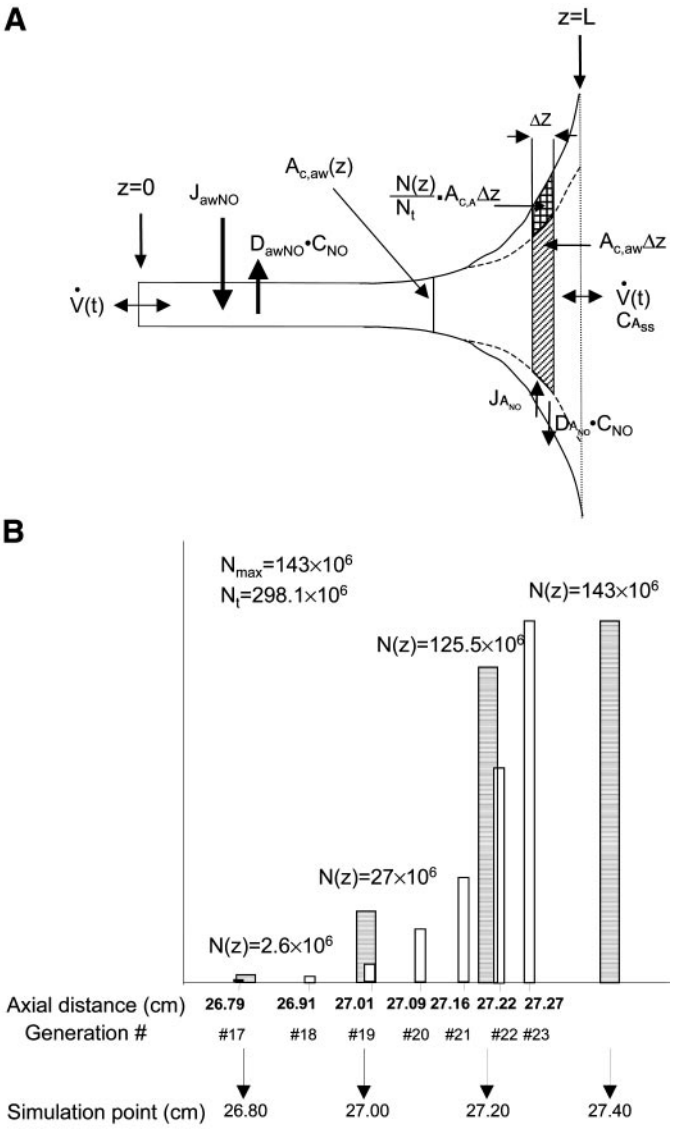

Fig. 1. *A*: schematic of the trumpet model based on the symmetrical bifurcating structure and anatomical data of Weibel (28). All parameters are identified in the *Glossary*. *B*: alveolar volume in the trumpet model is shown as a function of generation number and axial position. Open bar, no. of alveoli according to generation no. and axial position based on the anatomical data of Weibel. Shaded bar, no. of alveoli in the trumpet model with corresponding axial position.

the concentration [in parts per billion (ppb)] of NO in the airway gas phase (C_{NO}) is obtained from a mass balance over a differential volume of length Δz:

$$\left\{A_{c,aw}(z) + \left[\frac{N(z)}{N_t}\right]A_{c,A}\right\}\frac{dC_{NO}}{dt} = -\dot{V}\frac{dC_{NO}}{dz} + D_{NO,air}\frac{d}{dz}\left[A_{c,aw}(z)\frac{dC_{NO}}{dz}\right] + ((J'_{awNO} - D'_{awNO}C_{NO})\left[1 - \frac{N(z)}{N_{max}}\right] + (J'_{A_{NO}} - D'_{A_{NO}}C_{NO})\left[\frac{N(z)}{N_t}\right] \quad (1)$$

where $N(z)$ is the number of alveoli per unit axial distance [$N(z) = 0$ for $z < 26.8$ cm], N_{max} is the maximum number of alveoli per unit axial distance at any axial position (143×10^6), N_t is total number of alveoli in Weibel lung (298.1×10^6), $D_{NO,air}$ is the diffusion coefficient of NO in the gas phase (cm^2/s), $A_{c,aw}(z)$ is the cross-sectional area (cm^2) of the airway space, $A_{c,A}$ is the total cross-sectional area (cm^2) of the alveolar space, $\dot{V}$ is volumetric flow rate of air (cm^3/s), J'_{awNO} and $J'_{A_{NO}}$ are the maximum airway and alveolar fluxes per unit axial distance, respectively, of NO ($ppb \cdot ml \cdot s^{-1} \cdot cm^{-1}$), and D'_{awNO} and $D'_{A_{NO}}$ are the airway and alveolar diffusing capacities per unit axial distance, respectively ($ml \cdot s^{-1} \cdot cm^{-1}$). Units for J'_{awNO}, $J'_{A_{NO}}$, D'_{awNO}, and $D'_{A_{NO}}$ are described in greater detail in the GLOSSARY. The trumpet is assumed to be rigid; thus $A_{c,aw}(z)$ and $A_{c,A}$ are not a function of time. Air passes through the trumpet on inspiration at $z = 0$ and is assumed to exit the trumpet at $C_{A_{ss}}$. On exhalation, air enters the trumpet at z = length of airway in trumpet model (L) at $C_{A_{ss}}$. During both inspiration and expiration, the volumetric flow rate of air is assumed to be constant with respect to axial position.

The left-hand side of *Eq. 1* represents NO accumulation in the gas phase. The first term in the right-hand side of *Eq. 1* represents axial convection, the second term represents axial diffusion with variable cross-sectional area, the third term represents the airway production and adsorption rate of NO, and the last term represents the alveolar production and adsorption rate of NO. For $z < 26.8$ cm, there is no alveolar contribution to NO exchange, and $N(z) = 0$. This sets the fourth term on the right-hand side of *Eq. 1* to zero (no alveolar contribution), and the airway contribution includes the entire surface area, i.e., the term $[1 - N(z)/N_{max}] = 1$. For $z > 26.8$ cm, $N(z)$ progressively increases (see Fig. 1*B*) with z such that the magnitude of the third and fourth term on the right-hand side of *Eq. 1* decreases and increases, respectively. For example, at the end of the trumpet, $N(z) = N_{max}$, and there is no contribution from the airway source (i.e., $1 - N_{max}/N_{max} = 0$). The alveolar source at this axial position is the fraction of the alveolar surface area not utilized in the previous axial positions. The fraction is equal to $1 - N(z)/N_{max}$, which is $1 - 143 \times 10^6/298.1 \times 10^6 = 0.48$. In other words, 48% of the alveolar source of NO occurs at this axial position because of the fact that 48% of the alveoli are present or partitioned to this position. Radial velocity gradients are neglected (plug flow), and only the exchange of NO is considered. J_{awNO}, D_{awNO}, J_{ANO}, and D_{ANO} are assumed to be constant and uniformly distributed per unit volume.

Model solution. The governing equation is solved numerically using the method of lines (16, 20). This method uses a finite difference relationship for the spatial derivatives and ordinary differential equations for the time derivative. Thus, to seek $C_{NO}(z,t)$ that satisfies the governing equation, the airway is divided into K sections with K+1 node points in the axial position (z-coordinate). Each node is separated by a 0.2-cm interval (a smaller interval of 0.1 cm interval did not affect the solution; see APPENDIX). The first node is just before the mouth ($z = 0^-$), and the last node point ($z = L$) represents the end of the alveolar sacs. Then, a stiff integration algorithm including error estimation and time step-size control is used to ensure accuracy of the solution (16, 20). In all simulations, the accuracy of the independent variable (t) was set to 1.0×10^{-5}, and the requested maximal error tolerance for the dependent variable, C_{NO}, was 1.0×10^{-7}.

There is assumed to be no flux of NO across the end of the alveolar sacs (axial gradient is zero), which is equivalent to assuming equilibrium between alveolar NO production and adsorption. This has been shown to be a good assumption for exhalations that last >10 s, including any breath-hold time (5, 24). The airway is assumed initially to have a uniform zero NO concentration.

Because Weibel's symmetrical bifurcating model utilizes a generation number within the transition (*generations 17–19*) and respiratory (*generations 17–23*) regions, we sought values for $N(z)$ that would provide a similar distribution of alveolar space over the same axial dimensions. This is detailed in Fig. 1*B*, where the open bars represent the number of alveoli at the generation number and axial position in the Weibel model, and the shaded bars represent the number of alveoli and axial position (0.2-cm intervals) in our trumpet model. Additional details regarding the boundary conditions and numerical solution are in the APPENDIX.

Experimental data and model simulation. To simulate a series of different breathing maneuvers, we utilized previously estimated values for the flow-independent NO parameter values from the two-compartment model: J_{awNO} ($ppb \cdot ml \cdot s^{-1}$ or pl/s) = 640; D_{awNO} (ml/s or $pl \cdot s^{-1} \cdot ppb^{-1}$) = 4.2; J_{ANO} ($ppb \cdot ml \cdot s^{-1}$ or pl/s) = 3,638; D_{ANO} (ml/s or $pl \cdot s^{-1} \cdot ppb^{-1}$) = 1,467 (17, 25). Note that $C_{A_{ss}} = J_{ANO}/D_{ANO}$. We determined the impact of axial diffusion on NO gas exchange by performing simulations in the presence ($D_{NO,air} = 0.23$ cm^2/s) or in the absence ($D_{NO,air} = 0$) of axial diffusion. We then compared the performance of the model to two different types of experimental breathing maneuvers in the literature.

Breathing maneuver 1 is a single exhalation (vital capacity maneuver) preceded by a 20-s breath hold in which the exhalation flow rate decreases approximately linearly in time. This maneuver was first described by our group (26) and can be used to estimate D_{awNO}, J_{awNO}, and $C_{A_{ss}}$ from a single breathing maneuver. We combined the experimental breathing maneuvers from 10 healthy adults (each repeated five times) as previously reported (17) into a single composite profile representative of healthy adults. The exhalation flow rate decreases approximately linearly in time with an average relationship equal to $200 - 10 \times t$ (ml/s) where t is time (s) and the total expiratory time is 15 s.

For *breathing maneuver 1*, we are interested in predicting the dynamic shape of the profile. Consistent with our previous approach, this will include the volume of NO exhaled in phases I and II of the exhalation profile and the dynamic shape of phase III (17, 18, 26). The volume of NO that accumulates in the airways during the breath hold has previously been characterized by the area under curve in phases I and II ($A_{I,II}$) of the exhalation profile (Fig. 2*A*) (17, 18, 26). The boundaries of phases I and II in the exhalation profile are defined as the start of exhalation ($\dot{V}_E > 0$) and when the slope of exhaled concentration with time is equal to zero (26).

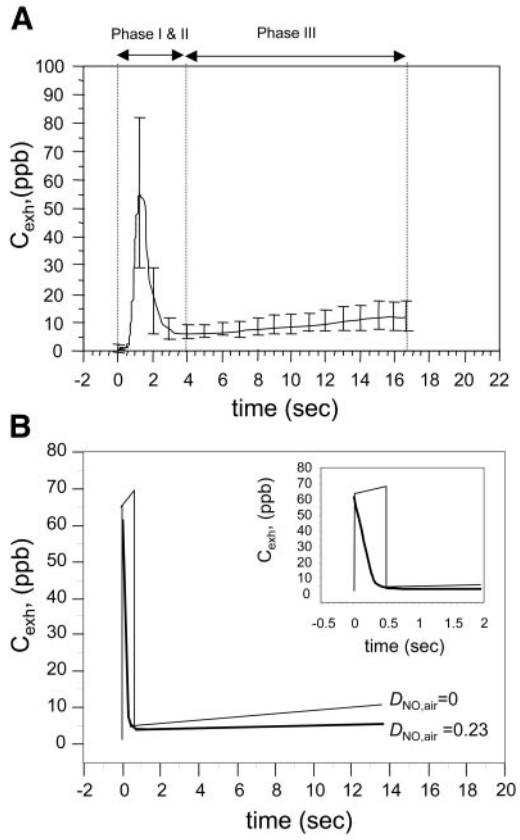

Fig. 2. *A*: composite experimental NO exhalation profile with standard deviation for *breathing maneuver 1* (20-s breath hold followed by a decreasing exhalation flow rate) for 10 healthy adults (17). *B*: model-predicted NO exhalation profiles for *breathing maneuver 1* in the absence (thin line) and presence (thick line) of axial diffusion. *Inset*, reduced time scale to highlight phases I and II of the exhalation profile. See *Glossary* for definitions. ppb, parts per billion.

Consistent with our previous report, the root mean square error (RMS) will be used as an index of the goodness of fit for the dynamic shape of phase III

$$\mathrm{RMS} = \sqrt{\sum_{i=1}^{n_{III}} (C^*_{exh,i} - C_{exh,i})^2 / n_{III}} \qquad (2)$$

where n_{III} is the number of data points in phase III and C^*_{exh} is the experimentally measured exhaled concentration of NO from the composite profile. Phases I, II, and III are identified in Fig. 2*A*.

Breathing maneuver 2 is a vital capacity maneuver without a breath hold in which the exhalation flow rate is held constant. We will examine data from our group at both 50 and 250 ml/s, as recommended by the American Thoracic Society (ATS) (1) and the European Respiratory Society (6), respectively, and also that reported by Silkoff et al. (22) over a much wider range of flow rates (4.2–1,550 ml/s). In this case, we are interested in predicting the plateau exhaled concentration (C_{NOplat}) in phase III (alveolar plateau) of the exhalation profile.

For both breathing maneuvers, inspired volume is assumed to be 4 liters at an inspiration flow rate of 2 l/s. In all cases, the experimentally reported value will have an asterisk (*). For example, the experimentally determined area under the curve in phases I and II will be denoted $A^*_{I,II}$.

RESULTS

Fig. 2*A* is the experimental composite exhalation profile for *breathing maneuver 1* (17). Fig. 2*B* presents the corresponding simulations of the trumpet model in the presence and absence of axial diffusion. Note that, in the absence of axial diffusion, the trumpet model is able to reproduce both $A_{I,II}$ and the dynamic shape of phase III (RMS = 0.94 ppb). This is an important feature of the performance of the trumpet model compared with the two-compartment model that was used to estimate the values used for D_{awNO}, J_{awNO}, D_{ANO}, and J_{ANO} used in the simulation. In the presence of axial diffusion, the peak value of NO in phases I and II is not affected; however, $A_{I,II}$ is reduced by ~50%, the concentration in phase III is reduced by a similar magnitude (concentration at end exhalation is reduced from 12.4 ppb to 6.24 ppb), and RMS in phase III increases to 3.0 ppb.

C_{NOplat} is presented in Fig. 3 for *breathing maneuver 2*. Both experimental and trumpet-model predicted values are shown in the presence and absence of axial diffusion. C_{NOplat}, using the trumpet model in the absence of axial diffusion, matches the experimental values over a wide range of exhalation flow rates consistent with the performance of the two-compartment model. However, in the presence of axial diffusion, C_{NOplat} as predicted by the trumpet model is significantly reduced. This effect is particularly exaggerated at lower flow rates.

Figure 4 presents the dynamic features of NO accumulation and elimination for *breathing maneuver 1* (inspiration, a 20-s breath hold, and expiration) in the absence (Fig. 4*A*) and presence (Fig. 4*B*) of axial diffusion. In the absence of axial diffusion, NO accumulates uniformly (*generations 0*, *12*, and *16* are indistinguishable) within the airways in an exponential fashion (24)

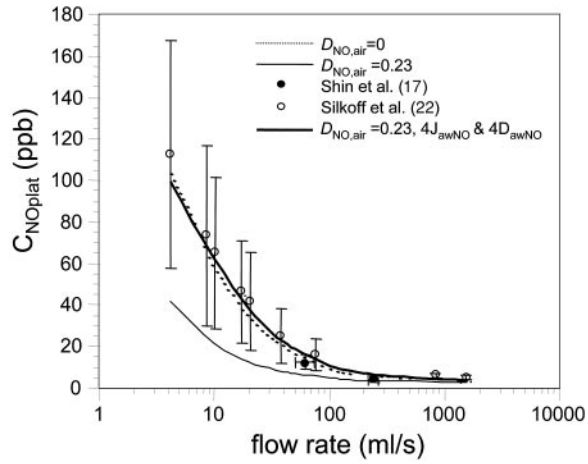

Fig. 3. C_{NOplat} as a function of constant exhalation flow rates. Experimental data points are presented as either open circles (22) or solid circles (17). Error bars represent SD. Dashed line is the 2-compartment model prediction in the absence of axial diffusion. Thin and thick solid line represents the trumpet-shaped airway model prediction in the presence of axial diffusion using the parameter values in *Experimental Data and Model Simulation*, and with J_{awNO} and D_{awNO} increased 4-fold. See *Glossary* for definitions.

during the breath hold. On exhalation, the width of phases I and II is relatively broad, reflecting significant NO levels throughout the airways. In the presence of axial diffusion, the concentration of NO in *generations 12* and *16* again increases in an exponential fashion but approaches a smaller concentration compared with when axial diffusion is neglected. The concentration at the end of the trumpet (*generation 23*) does not change during the breath hold, indicating a steady-state concentration in the alveolar region of ~2–3 ppb. On exhalation, the peak value (*generation 0*) is not changed, but the width of phases I and II is narrowed, reflecting lower concentrations of NO in the smaller airways. This finding is consistent with a smaller $A_{I,II}$ as previously described.

Figure 5 is the axial NO concentration in the airways just before exhalation ($t = 0$ s) and at end exhalation ($t = 15$ s) for *breathing maneuver 1* in the presence and absence of axial diffusion. Axial diffusion does not affect (<10% change) the NO concentration in the first 10 generations ($z < 25$ cm) at the end of the breath hold. For $z > 25$ cm, the NO concentration begins to decrease in the presence of axial diffusion such that the concentrations in *generations 12* ($z = 25.78$ cm) and *16* ($z = 26.65$ cm) are reduced by 18 and 50%, respectively. At end expiration, the exhaled concentration ($z = 0$) is significantly reduced in the presence of axial diffusion, consistent with Fig. 2*B*, and the concentration along the airways remains lower until approximately $z = 22.5$ cm. For $z > 22.5$ cm, the NO concentration in the airways is larger in the presence of axial diffusion.

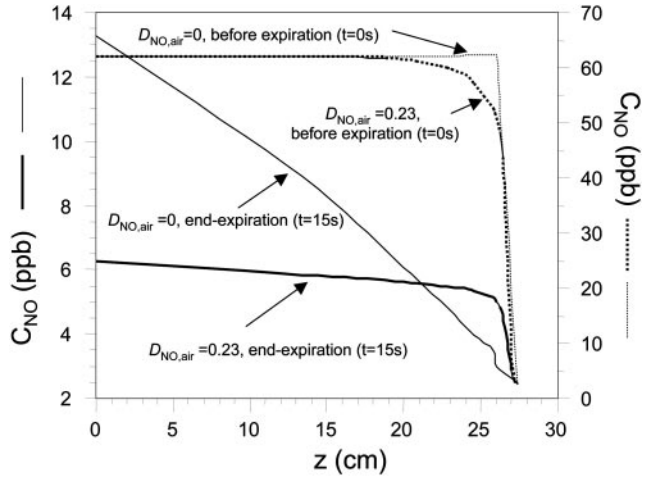

Fig. 5. Model-predicted NO concentration at the end of the 20-s breath hold ($t = 0$ s, dotted lines) and at end expiration ($t = 15$ s, solid line) as a function of the axial distance into the lungs. Dark lines are in the presence of axial diffusion and light lines are in the absence of axial diffusion. See *Glossary* for definitions.

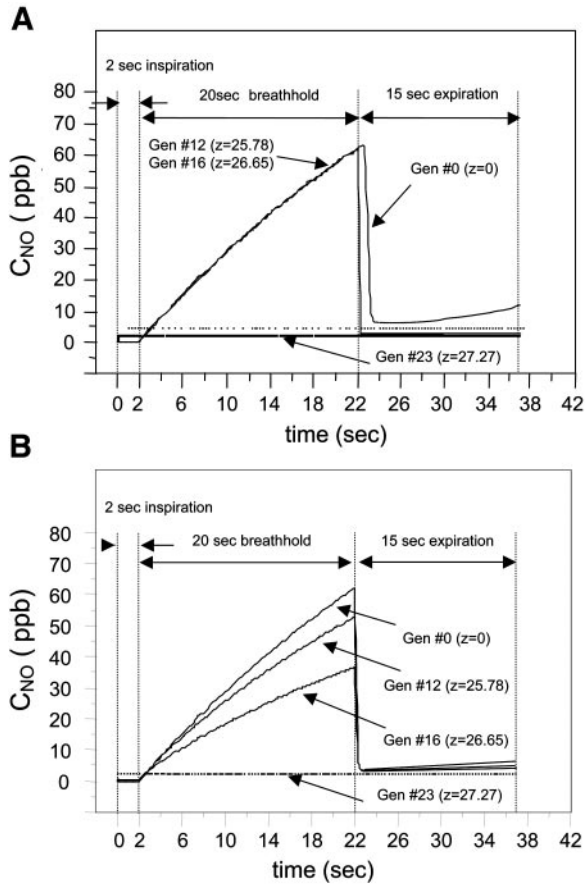

Fig. 4. Dynamic features of nitric oxide (NO) accumulation and elimination during inspiration, 20-s breath hold, and expiration are presented in the absence (*A*) and presence (*B*) of axial diffusion, respectively. Also shown are the NO concentrations at several different axial positions within the lungs [*generations (Gen#) 0*, *12*, *16*, and *23*]. See *Glossary* for definitions.

Figure 6 presents $A_{I,II}$, RMS, and C_{NOplat} for the two breathing maneuvers for a series of trumpet-model-simulated cases in which airway and alveolar compartment parameters are varied. Each parameter is normalized by a "gold standard" such that a value on the *y*-axis of unity is optimal. $A_{I,II}$ is normalized by the experimental value shown in Fig. 2*A*. RMS is normalized by the minimal (or optimal) value obtained by the two-compartment model as previously reported (17). C_{NOplat} is shown for an exhalation flow rate of ~50 ml/s (61.6 ml/s, from Ref. 19), which was the mean experimental value previously reported in 10 healthy adults and is approximately equal to the ATS guidelines. The goal is to estimate the impact of axial diffusion on previous estimates of flow-independent parameters by simultaneously simulating the experimentally observed NO exchange dynamics from both breathing maneuvers.

The first two bars in Fig. 6 represent the trumpet model in the absence and presence of axial diffusion, respectively, when the parameter values described above in *Experimental data and model simulation* are used. The next four bars represent the trumpet-model prediction in the presence of axial diffusion when J_{ANO}, D_{ANO}, J_{awNO}, and D_{awNO} are each increased fourfold. The last bar represents the trumpet-model prediction in the presence of axial diffusion when both J_{awNO} and D_{awNO} are increased fourfold. This provides a measure

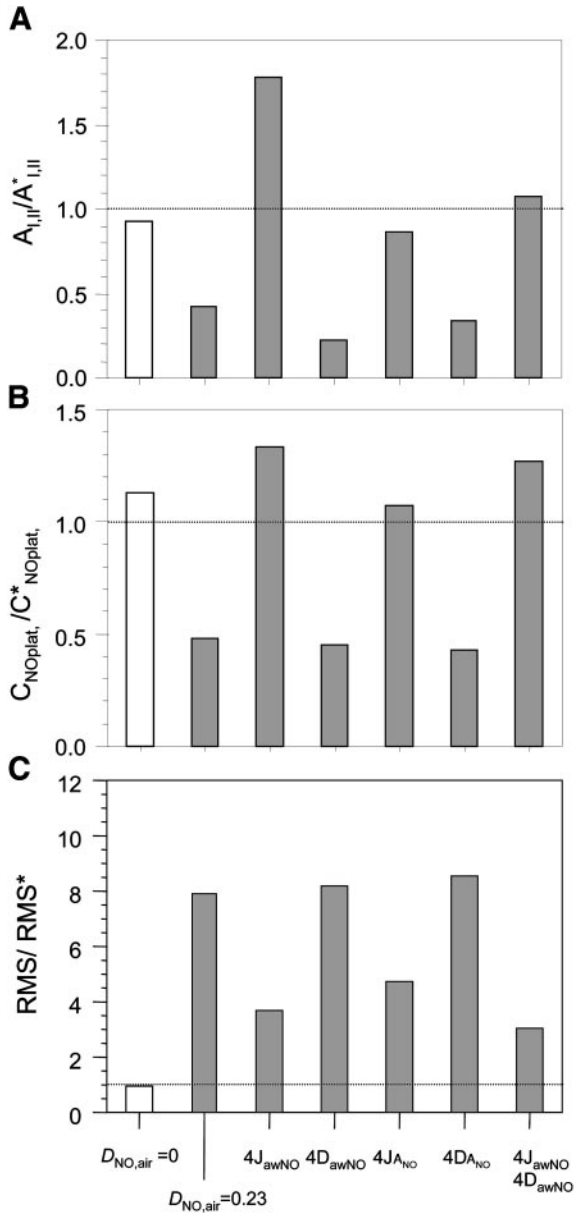

Fig. 6. Three indexes of model performance relative to experimental observations are shown as a function of different combinations of values for the flow-independent parameters. Open bar is in the absence of axial diffusion ($D_{NO,air}$ = 0), and solid bars are in the presence of axial diffusion ($D_{NO,air}$ = 0.23). Dotted lines are a value of unity representing the optimal value for each variable on the *y*-axis. *A*: area under the curve in phases I and II is normalized by the experimental area under the curve in Fig. 2*A*. *B*: plateau NO concentration at an exhalation flow rate of ~50 ml/s is normalized by the experimental value previously reported (19). *C*: RMS error in phase III is normalized by the optimal RMS error predicted by the 2-compartment model as previously reported (19). Asterisks denote experimentally reported values. See *Glossary* for definitions.

of the sensitivity of each of the experimental endpoints to the model parameters and represents a method by which we can describe general trends on the impact of axial diffusion on the estimated of the flow-independent NO parameters.

Relative to the case in the presence of axial diffusion (second bar in Fig. 6), if J_{ANO} is increased, $A_{I,II}$ is increased to a value near the experimentally observed value, RMS is decreased slightly, and C_{NOplat} is increased to near experimentally observed values. If D_{ANO} is increased, $A_{I,II}$ is unaffected, RMS increases slightly, and C_{NOplat} decreases slightly. If J_{awNO} is increased, $A_{I,II}$ is increased to a value above that observed experimentally, RMS is decreased, and C_{NOplat} is increased to near the experimentally observed value. If D_{awNO} is increased fourfold, $A_{I,II}$ is decreased, and the RMS and C_{NOplat} are essentially unaffected. The last bar represents the case where both J_{awNO} and D_{awNO} are increased fourfold. In this case, both $A_{I,II}$ and C_{NOplat} are changed to near experimental values, and the RMS is also significantly decreased. In addition, when both J_{awNO} and D_{awNO} are increased fourfold, C_{NOplat} is also accurately predicted over the entire range of constant exhalation flow rates as shown in Fig. 3.

Figure 7 is the simulated exhalation NO profile for *breathing maneuver 1* with a fourfold increase in both J_{awNO} and D_{awNO} (*case 4*) and also the case in which J_{ANO} is increased fourfold (*case 3*). The presence of axial diffusion with a fourfold increase in both J_{awNO} and D_{awNO} (*case 4*) forces phases I and II to be taller and narrower than in the absence of axial diffusion (*case 1*) while keeping $A_{I,II}$ constant. A fourfold increase in J_{ANO} (*case 3*) uniformly (in time) increases

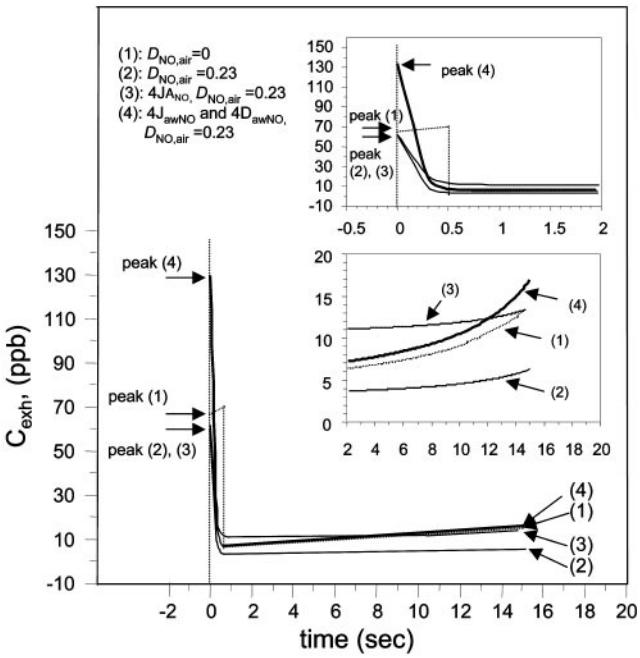

Fig. 7. Model-predicted NO exhalation profiles from *breathing maneuver 1* (20-s breath hold followed by a decreasing flow rate) are presented for 4 different cases: (*1*) in the absence of axial diffusion, (*2*) in the presence of axial diffusion, (*3*) with alveolar maximum flux increased 4-fold, and (*4*) and with airway maximum flux and airway diffusing capacity increased 4-fold. Insets represent different scales for the *x*-axis to highlight either phases I and II (*top*) or phase III (*bottom*). See *Glossary* for definitions.

the exhaled concentration in phase III, whereas a fourfold increase in both J_{awNO} and D_{awNO} (*case 4*) increases primarily the latter portion of phase III and is more consistent with experimental observations.

DISCUSSION

The currently accepted model of NO gas exchange divides the lungs into two compartments: the airways, in which convection is the dominant transport mechanism, and the alveolar region, which is assumed well mixed. Axial diffusion as a mechanism of transport in the gas phase has been neglected for simplicity. This study has incorporated axial diffusion into a one-dimensional trumpet model of lungs to describe gas-exchange dynamics of NO in the lungs. The explicit purpose was to determine the potential impact of axial diffusion on NO exchange dynamics, particularly on the estimation of flow-independent parameters that have been used to characterize the airway and alveolar compartments. We determined that axial diffusion results in the transport of NO toward the alveoli and thus decreases the elimination of NO in the exhaled breath. The loss of NO leads to potentially underestimating both the maximum airway flux and the airway diffusing capacity for NO in models that neglect axial diffusion; however, this conclusion is strongly dependent on a significant source of NO production in the small airways.

Impact of axial diffusion on phases I and II of exhaled NO profile. Our previously described two-compartment model neglected axial diffusion and could not accurately predict the shape of the exhalation NO profile in phases I and II after a breath hold (17, 18, 26). In these reports, we suggested that axial diffusion was a potential cause, and we used the model to predict the area under the curve in phases I and II rather than the precise shape. When axial diffusion was included in the trumpet model in the present study, the shape of phases I and II was substantially altered (narrower width with a sharper peak and smoother transition to phase III); however, the shape still does not match that of the experimental data (Fig. 2). The experimentally observed shape of phases I and II remains broader (nearly 4 s compared with the model-predicted value of 2 s for the same exhalation flow rate). Thus it is apparent that additional mechanisms of gas mixing are still neglected in this simple one-dimensional model, which may be important to fully describe NO exchange mechanisms.

One important possibility is ventilation to volume heterogeneity, which results in different regions of lungs filling and emptying at different rates. During exhalation, regions of the lungs with lower concentrations (high ventilation-to-volume ratio) tend to empty first. This contributes to the positive phase III slope of inert gases, as well as phase II (transition from conducting airway space to the alveolar plateau) of the inert-gas exhalation profile (11). The impact of ventilation to volume heterogeneity on the estimation of the flow-independent parameters is not known and is a potential topic of future studies. A second possibility is the impact of a changing airway cross-sectional area during inhalation and exhalation. Our simple trumpet model assumes a rigid geometry with an effective mean value for $A_{c,aw}(z)$ and $A_{c,A}$ equal to that of the lungs utilized by Weibel (28), which were fixed at ~75% total lung capacity. In fact, during the breath hold at total lung capacity, $A_{c,aw}(z)$ and $A_{c,A}$ will be slightly larger, thus enhancing axial diffusion. Therefore, our predictions are likely to be a conservative estimate of the impact of axial diffusion.

The observation that axial diffusion narrows the width of phases I and II without affecting the peak value (Fig. 2*B*) results in less NO being eliminated in this portion of the exhaled profile. Estimation of J_{awNO} and D_{awNO} is sensitive to the volume of NO eliminated in the phases I and II peak after a breath hold (26). This is evident by analyzing *Eq. 1*, which demonstrates that the flux of NO into the airway space from the airway wall is the difference between J_{awNO} and $D_{awNO} \cdot C$ (third term on right-hand side). At very small flow rates (<50 ml/s), the concentration in the gas phase increases (Fig. 3); thus the product $D_{awNO} \cdot C$ becomes important in determining the concentration in the gas phase. At higher flow rates, the exhaled concentration depends mainly on J_{awNO}; thus estimation of D_{awNO} depends solely on phases I and II, whereas estimation of J_{awNO} depends on all three phases.

Impact of axial diffusion on phase III of exhaled NO profile. The concentration of NO in phase III of the exhalation profile depends on the relative contributions from both the alveolar and airway compartments (26). At very high flow rates (>500 ml/s), the residence time of a volumetric element of gas (i.e., gas bolus) is small, and exhaled NO is predominantly from the alveolar region. The progressively increasing concentration in phase III of the NO exhalation profile for *breathing maneuver 1* is due primarily to the fact that the flow is decreasing linearly in time (Fig. 2*A*). Thus the alveolar contribution remains approximately constant (constant concentration in a collapsing balloon), whereas the contribution from the airways increases (larger residence time at slow flow rates). The presence of axial diffusion decreases the concentration of NO in phase III, but the effect is more exaggerated at lower flow rates (late portion of phase III, Fig. 2*B* and Fig. 3). If axial diffusion were primarily affecting the alveolar concentration, the impact on phase III would be uniform. For example, if the alveolar concentration increased by 5 ppb, then the entire phase III concentration would uniformly increase by 5 ppb. This is not the observed effect. It is clear from Fig. 2*B* and Fig. 3 that axial diffusion has a greater effect at smaller flow rates. In addition, although increasing J_{ANO} by fourfold increases the end-exhaled NO concentration and thus compensates for the loss of NO due to axial diffusion, this change does not significantly improve the RMS in phase III (Fig. 6*C*).

The relationship between the impact of axial diffusion and exhalation flow rate is best understood by comparing the velocity of axial convection to the velocity of diffusion. This ratio is captured in the dimensionless Peclet number (Pe) defined by:

$$\mathrm{Pe} = \frac{4\dot{V}_E/\pi D^2}{D_{NO,air}/L} = \frac{\text{velocity of convection}}{\text{velocity of diffusion}} \qquad (3)$$

where D and L are the diameter and length of the airway, respectively. For Pe = 1, convection and diffusion are of equal magnitude. Fig. 8 presents Pe as a function of axial distance into the airways for constant exhalation flow rates of 50 and 250 ml/s. As the flow rate increases, a larger portion of the airways is dominated by convection, and axial diffusion plays a smaller role. According to Fick's first law of diffusion, axial diffusion is proportional to the concentration gradient and is in the opposite direction of the gradient. It is evident from Fig. 5 that the concentration gradient in NO within airways is negative (concentration decreases as axial position increases); thus axial diffusion of NO is toward the alveoli (positive z-direction) and in the opposite direction of convection during expiration. This "backdiffusion" of NO toward the alveolar region results in loss of the NO to the pulmonary blood.

Impact of axial diffusion on flow-independent NO exchange parameters. It is evident that the presence of axial diffusion results in loss of NO to the alveolar region (Figs. 4 and 5). Thus, in order for the trumpet model to simulate the experimentally observed exhaled NO concentrations, the endogenous sources of NO (i.e., J_{ANO} and J_{awNO}) need to be increased. We used three experimental endpoints ($A_{I,II}$, RMS, and C_{NOplat}) from two different breathing maneuvers that included all three phases of the exhalation to estimate the potential impact of axial diffusion on flow-independent parameters (Fig. 6). It was evident that both J_{ANO} and J_{awNO} could increase exhaled NO concentration; however, only increasing J_{awNO} compensated for the impact on all three phases (phases I and II are insensitive to alveolar NO production).

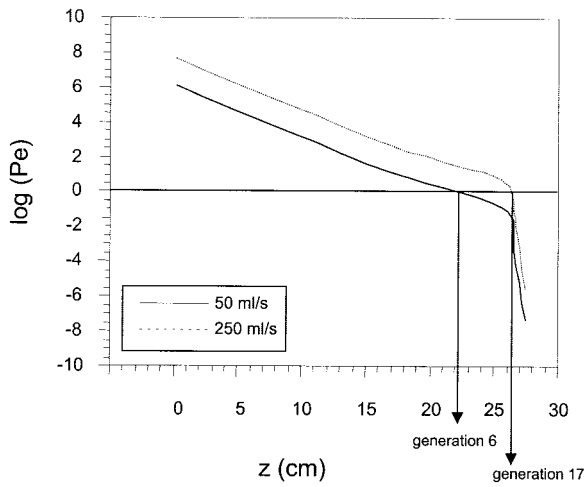

Fig. 8. Log Peclet number (Pe) is shown as a function of axial distance into the lungs at either an exhalation flow rate of 50 ml/s (solid line) or 250 ml/s (dotted line). Line at log(Pe) = 0 represents the position in the lungs where axial diffusion and convection are of equal magnitude.

We then observed that a fourfold increase in J_{awNO} was needed to simulate phase III, but this caused too large an increase in the area of phases I and II. Thus one could compensate for this by increasing consumption in the airways by increasing D_{awNO} by fourfold without affecting phase III (flow rates are large enough during phase III in *breathing maneuver 1* that NO concentration in phase III is insensitive to D_{awNO}). In summary, a fourfold increase in both J_{awNO} and D_{awNO} compensates for the effects of axial diffusion in all three phases of the exhalation profile over a wide range of exhalation flow rates (Figs. 3 and 6). The obvious question becomes: are these predicted increases possible or reasonable?

Our laboratory has previously shown (24, 25) that J_{awNO} depends on the physical dimensions of the airway such as surface area and tissue thickness but is also a positive function of the production rate of NO per unit volume. Thus one possibility is simply a larger production rate of NO per unit volume of tissue to account for the possible increase in J_{awNO}.

The potential impact of axial diffusion on D_{awNO} is more difficult to understand or justify. Our laboratory has demonstrated previously (24) that the diffusing capacity of a gas produced within the tissue (either airway or alveolar) can be estimated by the relatively simply expression:

$$D_{awNO} = \frac{A_{aw}\lambda_{ti,air}D_{NO,ti}}{L_{ti}} \cdot \frac{\xi}{\tanh(\xi)} \qquad (4)$$

where $\lambda_{ti,air}$ is the tissue-air partition coefficient of NO, A_{aw} (cm^2) is the surface area available for diffusion, $D_{NO,ti}$ (cm^2/s) is the molecular diffusivity of NO in the tissue, L_{ti} is the thickness of the tissue layer, $\xi = \sqrt{k/(D_{NO,ti}/L_{ti}^2)}$, and k (s^{-1}) is the first-order rate constant that characterizes the rate of chemical consumption by substrates such as superoxide. The ξ represents a dimensionless ratio of the rate of chemical consumption to the rate of molecular diffusion. When consumption of the gas is negligible relative to diffusion (k approaches zero), $\xi/\tanh(\xi)$ approaches unity, and D_{awNO} approaches the more familiar definition of the diffusing capacity of an inert gas. When diffusion is negligible (i.e., k becomes large), $D_{awNO} = A_{aw}\lambda_{ti,air}\sqrt{D_{NO,ti}k}$. The hyperbolic tangent (tanh) is bounded between -1 and 1 and is a monotonically increasing function of its argument. From *Eq. 4*, D_{awNO} is a positive function of A_{aw}, $\lambda_{ti,air}$, $D_{NO,ti}$, and k, and it is an inverse function of L_{ti}. *Eq. 4* provides units of ml/s for D_{awNO}, which are equivalent to $pl \cdot s^{-1} \cdot ppb^{-1}$.

Representative values for A_{aw}, L_{ti}, $\lambda_{ti,air}$, $D_{NO,ti}$, and k are 9,100 cm^2, 0.002 cm, 0.0412, 0.000033 cm^2/s, and 0.69 s^{-1} ($\xi = 0.29$) based on Weibel's symmetrical structure (28), reported values in the literature, and a half-life of NO in vivo of ~1 s (18, 24, 25), respectively.

Using *Eq. 4*, a value of 6.35 ml/s ($pl \cdot s^{-1} \cdot ppb^{-1}$) is produced for D_{awNO}, which is very close to the values used in the simulations as well as others using a two-compartment model without axial diffusion. To increase D_{awNO} fourfold (~20–25 ml/s), one would need to justify appropriate changes (from values presented above) in one or more of these physical parameters. A further decrease in L_{ti} or increase in A_{aw} seems unreasonable because they are already at their realistic limits. $D_{NO,ti}$ and $\lambda_{ti,air}$ are well-characterized physical parameters and not likely to vary much from the values reported above; k is not well characterized, and the dependence of D_{awNO} on k is highly nonlinear. For $k < 1$, D_{awNO} is essentially independent of k (*Eq. 4*); however, for $k > 1$, D_{awNO} becomes a strong positive function. Nonetheless, in order for D_{awNO} to attain values on the order of 20 ml/s, k would need to be ~70 s^{-1} or a half-life of <0.01 s. This does not seem plausible on the basis of reported reaction rates of NO with substrates present in lung tissue (19). Hence, on the basis of anatomical and physical constraints in the lungs, it is difficult to justify values for D_{awNO} greater than 5–10 ml/s (as opposed to the prediction of 20–25 ml/s predicted by the trumpet model).

One possible solution to this dilemma is the fact that the contribution of the small airways to exhaled NO when J_{awNO} and D_{awNO} have been increased fourfold in the presence of axial diffusion remains too large compared with experimental observations. Silkoff et al. (21) have reported that ~50% of NO arises from the upper airways (*generations 0–2*). In the present simulation using the trumpet model, the NO concentration at end expiration of the single-breath maneuver in *generation 2* (z = 18.7 cm) is 52% (see Fig. 5) of the exhaled NO concentration (z = 0 cm) in the absence of axial diffusion (i.e., consistent with Silkoff et al.). However, in the presence of axial diffusion, independent of increasing J_{awNO} and D_{awNO} by fourfold, the concentration at *generation 2* increases to >85% of exhaled NO concentration (z = 0 cm). Thus the trumpet model in the presence of axial diffusion predicts too much NO production in the smaller airways. It is possible that distributing D_{awNO} and J_{awNO} uniformly per unit airway volume may not truly represent the axial distribution of NO production and diffusion in the airways. Future theoretical studies must address these important issues to formulate a complete understanding of the impact of axial diffusion on the estimation of flow-independent NO exchange parameters.

In conclusion, previous models aimed at characterizing NO pulmonary exchange dynamics have neglected axial diffusion as a transport mechanism. This study has incorporated axial diffusion into a one-dimensional trumpet model of NO gas exchange in the lungs. We demonstrated that, in the absence of the axial diffusion, the trumpet model behaves very similarly to the two-compartment model. In the presence of axial diffusion, the trumpet model predicts a significant back-diffusion of NO from the airways into the alveolar region. This results in a significant loss of NO that would, therefore, not appear in the exhaled breath. The result is a potential underestimation of both the maximum airway flux of NO and the airway diffusing capacity for NO. This result hinges on a significant production of NO in the very small airways, for which there is evidence to the contrary. Future theoretical work must focus on incorporating more advanced features of NO gas exchange consistent with experimental observations, such as spatial heterogeneity in alveolar concentration and airway NO production, before the true impact of axial diffusion can be determined.

APPENDIX

Governing equation. The unsteady-state simultaneous convection-diffusion equation from the trumpet-shaped Weibel lung (Fig. 1) is derived by the following NO mass balance and a total mass balance, respectively, over a differential length Δz:

NO mass balance

$$\frac{d}{dt}\left(C_{NO}\{A_{c,aw}(z) + \left[\frac{N(z)}{N_t}\right]A_{c,A}\}\Delta z\right) = [\dot{V}C_{NO}|_{z+\Delta z}^{z}] - D_{NO,air}\left[A_{c,aw}(z)\frac{dC_{NO}}{dz}\bigg|_{z+\Delta z}^{z}\right] + (J'_{awNO} - D'_{awNO}C_{NO}) \times \left[1 - \frac{N(z)}{N_{max}}\right]\Delta z + (J'_{A_{NO}} - D'_{A_{NO}}C_{NO})\left[\frac{N(z)}{N_t}\right]\Delta z \quad (A1)$$

Total mass balance

$$\frac{d}{dt}\left(\rho\left\{A_{c,aw}(z) + \left[\frac{N(z)}{N_t}\right]A_{c,A}\right\}\Delta z\right) = [\rho\dot{V}|_{z+\Delta z}^{z}] \quad (A2)$$

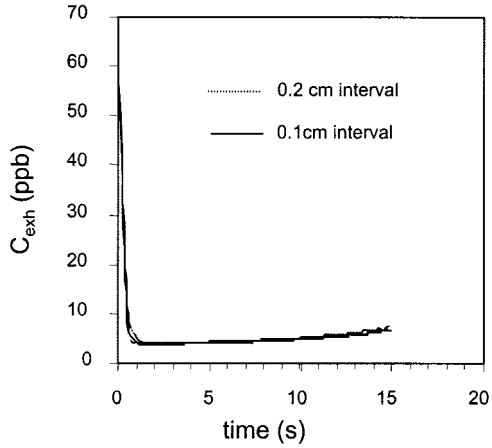

Fig. A1. Model simulation of *breathing maneuver 1* (20-s breath hold followed by a decreasing exhalation flow rate) in which 2 different interval sizes are utilized in the numerical solution (0.1 cm and 0.2 cm). See *Glossary* for definitions.

Expanding derivatives of products and division of *Eqs. A1* and *A2*, respectively, by Δz, then letting $\Delta z \rightarrow 0$ produces

$$\left(\left\{A_{c,aw}(z) + \left[\frac{N(z)}{N_t}\right]A_{c,A}\right\}\frac{dC_{NO}}{dt}\right) + C_{NO}\frac{d}{dt}\left\{A_{c,aw}(z) + \left[\frac{N(z)}{N_t}\right]A_{c,A}\right\} = -\left(\dot{V}\frac{dC_{NO}}{dz} + C_{NO}\frac{d\dot{V}}{dz}\right) + D_{NO,air}\frac{d}{dz}\left[A_{c,aw}(z)\frac{dC_{NO}}{dz}\right] + (J'_{awNO} - D'_{awNO}C_{NO})\left[1 - \frac{N(z)}{N_{max}}\right] + (J'_{A_{NO}} - D'_{A_{NO}}C_{NO})\left[\frac{N(z)}{N_t}\right] \quad (A3)$$

and

$$\frac{d}{dt}\left\{A_{c,aw}(z) + \left[\frac{N(z)}{N_t}\right]A_{c,A}\right\} = -\frac{d\dot{V}}{dz} \quad (A4)$$

Inserting the result from the total mass balance (*Eq. A4*) into the NO mass balance (*Eq. A3*) reduces *Eq. A3* to the governing equation presented in the main text (*Eq. 1*).

The initial condition for *Eq. 1* for inspiration is $C_{NO}(z,t = 0)$, and for expiration it is equal to the concentration profile just before exhalation (either after the 20-s breath hold for *breathing maneuver 1* or end inspiration for *breathing maneuver 2*). The boundary conditions for *Eq. 1* are as follows

Inspiration

$$C_{NO}(z = 0^-,t) = 0 \text{ (ambient air zero concentration)} \quad (A5)$$

$$\frac{dC_{NO}(z = L,t)}{dz} = 0 \text{ (no flux at end of airway)} \quad (A6)$$

Expiration

$$\frac{dC_{NO}(z = 0^-,t)}{dz} = 0 \quad (A7)$$

$$\frac{dC_{NO}(z = L,t)}{dz} = 0 \text{ (no flux at end of airway)} \quad (A8)$$

where $z = 0^-$ refers to a single node just outside of the airway. This strategy allows a numerical solution. For example, *Eq. A6* arises as diffusion is negligible near the mouth ($z = 0$), and we assume a single node ($z = 0^-$) in which there is no diffusion of NO from the airway wall; thus the axial concentration gradient is zero.

Grid size in model solution. We determined that 0.2 cm was the minimum grid size necessary to understand the impact of axial diffusion on the exhaled NO profile by halving the interval size to 0.1 cm and demonstrating no significant impact on the exhaled NO profile. This is demonstrated in Fig. A1 in which the model-predicted exhaled NO profile, using the same parameters as that in Fig. 2*B*, is essentially identical at grid sizes of both 0.2 and 0.1 cm.

This work was supported by National Heart, Lung, and Blood Institute Grant HL-60636.

REFERENCES

1. **American Thoracic Society.** Recommendations for standardized procedures for the on-line and off-line measurement of exhaled lower respiratory nitric oxide and nasal nitric oxide in adults and children—1999. *Am J Respir Crit Care Med* 160: 2104–2117, 1999.
2. **Barnes PJ and Kharitonov SA.** Exhaled nitric oxide: a new lung function test. *Thorax* 51: 233–237, 1996.
3. **DuBois AB, Kelley PM, Douglas JS, and Mohsenin V.** Nitric oxide production and absorption in trachea, bronchi, bronchioles, and respiratory bronchioles of humans. *J Appl Physiol* 86: 159–167, 1999.
4. **Hogman M, Drca N, Ehrstedt C, and Merilainen P.** Exhaled nitric oxide partitioned into alveolar, lower airways and nasal contributions. *Respir Med* 94: 985–991, 2000.
5. **Hyde RW, Geigel EJ, Olszowka AJ, Krasney JA, Forster RE 2nd, Utell MJ, and Frampton MW.** Determination of production of nitric oxide by lower airways of humans—theory. *J Appl Physiol* 82: 1290–1296, 1997.
6. **Kharitonov S, Alving K, and Barnes PJ.** Exhaled and nasal nitric oxide measurements: recommendations. The European Respiratory Society Task Force. *Eur Respir J* 10: 1683–1693, 1997.
7. **Kobzik L, Bredt DS, Lowenstein CJ, Drazen J, Gaston B, Sugarbaker D, and Stamler JS.** Nitric oxide synthase in human and rat lung: immunocytochemical and histochemical localization. *Am J Respir Cell Mol Biol* 9: 371–377, 1993.
8. **Lehtimaki L, Kankaanranta H, Saarelainen S, Hahtola P, Jarvenpaa R, Koivula T, Turjanmaa V, and Moilanen E.** Extended exhaled NO measurement differentiates between alveolar and bronchial inflammation. *Am J Respir Crit Care Med* 163: 1557–1561, 2001.
9. **Lehtimaki L, Turjanmaa V, Kankaanranta H, Saarelainen S, Hahtola P, and Moilanen E.** Increased bronchial nitric oxide production in patients with asthma measured with a novel method of different exhalation flow rates. *Ann Med* 32: 417–423, 2000.
10. **Paiva M.** Boundary conditions and geometry in pulmonary gas transport models. *Comput Biomed Res* 13: 271–282, 1980.
11. **Paiva M and Engel LA.** The anatomical basis for the sloping N_2 plateau. *Respir Physiol* 44: 325–337, 1981.
12. **Pietropaoli AP, Perillo IB, Torres A, Perkins PT, Frasier LM, Utell MJ, Frampton MW, and Hyde RW.** Simultaneous measurement of nitric oxide production by conducting and alveolar airways of humans. *J Appl Physiol* 87: 1532–1542, 1999.
13. **Schedin U, Frostell C, Persson MG, Jakobsson J, Andersson G, and Gustafsson LE.** Contribution from upper and lower airways to exhaled endogenous nitric oxide in humans. *Acta Anaesthesiol Scand* 39: 327–332, 1995.
14. **Scherer PW, Gobran S, Aukburg SJ, Baumgardner JE, Bartkowski R, and Neufeld GR.** Numerical and experimental study of steady-state CO_2 and inert gas washout. *J Appl Physiol* 64: 1022–1029, 1988.
15. **Scherer PW, Shendalman LH, and Greene NM.** Simultaneous diffusion and convection in single breath lung washout. *Bull Math Biophys* 34: 393–412, 1972.
16. **Schiesser WE.** *The Numerical Method of Lines*. San Diego, CA: Academic, 1991.
17. **Shin HW, Rose-Gottron CM, Perez F, Cooper DM, Wilson AF, and George SC.** Flow-independent nitric oxide exchange parameters in healthy adults. *J Appl Physiol* 91: 2173–2181, 2001.
18. **Shin HW, Rose-Gottron CM, Sufi RS, Perez F, Cooper DM, Wilson AF, and George SC.** Flow-independent nitric oxide exchange parameters in cystic fibrosis. *Am J Respir Crit Care Med* 165: 349–357, 2002.
19. **Shin HY and George SC.** Microscopic modeling of NO and *S*-nitrosoglutathione kinetics and transport in human airways. *J Appl Physiol* 90: 777–788, 2001.
20. **Silebi CA and Schiesser WE.** *Dynamic Modeling of Transport Process Systems*. San Diego, CA: Academic, 1992.
21. **Silkoff PE, McClean PA, Caramori M, Slutsky AS, and Zamel N.** A significant proportion of exhaled nitric oxide arises in large airways in normal subjects. *Respir Physiol* 113: 33–38, 1998.

22. **Silkoff PE, McClean PA, Slutsky AS, Furlott HG, Hoffstein E, Wakita S, Chapman KR, Szalai JP, and Zamel N.** Marked flow-dependence of exhaled nitric oxide using a new technique to exclude nasal nitric oxide. *Am J Respir Crit Care Med* 155: 260–267, 1997.
23. **Silkoff PE, Sylvester JT, Zamel N, and Permutt S.** Airway nitric oxide diffusion in asthma: role in pulmonary function and bronchial responsiveness. *Am J Respir Crit Care Med* 161: 1218–1228, 2000.
24. **Tsoukias NM and George SC.** A two-compartment model of pulmonary nitric oxide exchange dynamics. *J Appl Physiol* 85: 653–666, 1998.
25. **Tsoukias NM and George SC.** Impact of volume-dependent alveolar diffusing capacity on exhaled nitric oxide concentration. *Ann Biomed Eng* 29: 731–739, 2001.
26. **Tsoukias NM, Shin HW, Wilson AF, and George SC.** A single-breath technique with variable flow rate to characterize nitric oxide exchange dynamics in the lungs. *J Appl Physiol* 91: 477–487, 2001.
27. **Watkins DN, Peroni DJ, Basclain KA, Garlepp MJ, and Thompson PJ.** Expression and activity of nitric oxide synthases in human airway epithelium. *Am J Respir Cell Mol Biol* 16: 629–639, 1997.
28. **Weibel ER.** *Morphometry of the Human Lung*. Berlin: Springer-Verlag, 1963.